Research Article | Vol. 25, No. 14 | 10 Jul 2017 | OPTICS EXPRESS 16214
Optics EXPRESS

Integrated Vivaldi plasmonic antenna for wireless on-chip optical communications

GAETANO BELLANCA,[1] GIOVANNA CALÒ,[2] ALI EMRE KAPLAN,[1] PAOLO BASSI,[3] AND VINCENZO PETRUZZELLI[2,*]

[1]*Department of Engineering, University of Ferrara, Via Saragat, 1, Ferrara, 44122, Italy*
[2]*Dipartimento di Ingegneria Elettrica e dell'Informazione, Politecnico di Bari, Via Orabona, 4, Bari, 70125, Italy*
[3]*Department of Electrical, Electronic and Information Engineering, University of Bologna, Viale del Risorgimento, 2, Bologna, 40136, Italy*
[*]*vincenzo.petruzzelli@poliba.it*

Abstract: In this paper we propose a novel hybrid optical plasmonic Vivaldi antenna for operation in the standard C telecommunication band for wavelengths in the 1550 *nm* range. The antenna is fed by a silicon waveguide and is designed to have high gain and large bandwidth. The shape of the radiation pattern, with a main lobe along the antenna axis, makes this antenna suitable for point-to-point connections for inter- or intra-chip optical communications. Direct port-to-port short links for different connection distances and in a homogeneous environment have also been simulated to verify, by comparing the results of a full-wave simulation with the Friis transmission equation, the correctness of the antenna parameters obtained via near-to-far field transformation.

OCIS codes: Optical antennas; (350.4238) Nanophotonics; (240.6680) Surface plasmons; (260.3910) Metal optics; (060.4510) Optical communications.

References and links

1. L. Benini and G. D. Micheli, "Networks on chips: a new SoC paradigm," Computer **35**(1), 70–78 (2002).
2. R. G. Beausoleil, P. J. Kuekes, G. S. Snider, S. Wang and R. S. Williams, "Nanoelectronic and nanophotonic interconnect," Proc. IEEE **96**(2), 230–247 (2008).
3. A. Shacham, K. Bergman and L.P. Carloni, "Photonic networks-on-chip for future generations of chip multiprocessors," IEEE Trans. Comput. **57**(9), 1246–1260 (2008).
4. D. B. Miller, "Device requirements for optical interconnects to silicon chips," Proc. IEEE **97**(7), 1166–1185 (2009).
5. A. Biberman and K. Bergman, "Optical interconnection networks for high-performance computing systems," Rep. Prog. Phys. **75**(4), 046402 (2012).
6. F. Gambini, S. Faralli, P. Pintus, N. Andriolli and I. Cerutti, "BER evaluation of a low-crosstalk silicon integrated multi-microring network-on-chip," Opt. Express **23**(13), 17169–17178, (2015).
7. E. Fusella and A. Cilardo, "Crosstalk-aware automated mapping for optical networks-on-chip," ACM Trans. Embedded Comput. Syst. **16**(1), 16.1–16.26 (2016).
8. M. Ortin-Obon, M. Tala, L. Ramini, V. Vinals-Yufera and D. Bertozzi, "Contrasting laser power requirements of wavelength-routed optical NoC topologies subject to the floorplanning, placement and routing constraints of a 3D-stacked system," IEEE Transactions Very Large Scale Integr. (VLSI) Syst. (posted 28 March 2017, in press).
9. J. Lin, H. Wu, Y. Su, L. Gao, J. E. Brewer and K. K. O, "Communication using antennas fabricated in silicon integrated circuits," IEEE J. Solid-State Circuits **42**(8), 1678–1687, (2007).
10. A. Ganguly, K. Chang, S. Deb, P. P. Pande, B. Belzer and C. Teuscher, "Scalable hybrid wireless network-on-chip architectures for multicore systems," IEEE Trans. Comput. **60**(10), 1485–1502 (2011).
11. S. Deb, A. Ganguly, P.P. Pande, B. Belzer and D. Heo, "Wireless NoC as interconnection backbone for multicore chips: promises and challenges," IEEE J. Emerg. Sel. Topic Circuits Syst. **2**(2), 228–239 (2012).
12. D. W. Matolak, A. Kodi, S. Kaya, D. Di Tomaso, S. Laha and W. Rayess, "Wireless networks-on-chips: architecture, wireless channel and devices," Wireless Commun. **19**(5), 58–65 (2012).
13. A. Alù and N. Engheta, "Wireless at the nanoscale: optical interconnects using matched nanoantennas," Phys. Rev. Lett. **104**, 213902 (2010).
14. Y. Yang, Q. Li and M. Qiu, "Broadband nanophotonic wireless links and networks using on-chip integrated plasmonic antennas," Sci. Rep. **6**, 19490 (2016).
15. J. M. Merlo, N.T. Nesbitt, Y.M. Calm, A.H. Rose, L. D'Imperio, C. Yang, J.R. Naughton, M.J. Burns K. Kempa and M.J. Naughton, "Wireless communication system via nanoscale plasmonic antennas," Sci. Rep. **6**, 31710 (2016).

#293442 https://doi.org/10.1364/OE.25.016214
Journal © 2017 Received 26 Apr 2017; revised 30 May 2017; accepted 31 May 2017; published 29 Jun 2017

Optics EXPRESS

16. D. M. Solís, J. M. Taboada, F. Obelleiro and L. Landesa, "Optimization of an optical wireless nanolink using directive nanoantennas," Opt. Express **21**(2), 2369–2377 (2013).
17. L. Novotny and N. Van Hulst, "Antennas for light," Nat. Photonics **5**, 83–90 (2011).
18. P. Bharadwaj, B. Deutsch and L. Novotny, "Optical antennas," Adv. Opt. Photonics **1**(3), 438–483 (2009).
19. E. M. Atie, Z. Xie, A. L. Eter, R. Salut and D. Nedeljkovic, "Remote optical sensing on the nanometer scale with a bowtie aperture nano-antenna on a fiber tip of scanning near-field optical microscopy," Appl. Phys. Lett. **106**, 151104 (2015).
20. D. Bar-Lev and J. Scheuer, "Efficient second harmonic generation using nonlinear substrates patterned by nanoantenna arrays," Opt. Express **21**(24), 29165–29178 (2013).
21. G. M. Akselrod, C. Argyropoulos, T. B. Hoang, C. Ciracì, C. Fang, J. Huang, D. R. Smith and M. H. Mikkelsen, "Probing the mechanisms of large Purcell enhancement in plasmonic nanoantennas," Nat. Photonics **8**, 835–840 (2014).
22. R. Guo, M. Decker, F. Setzpfandt, I. Staude, D. N. Neshev and Y. S. Kivshar, "Plasmonic Fano nanoantennas for on-chip separation of wavelength-encoded optical signals," Nano Lett. **15**(5), 3324–3328 (2005).
23. R. Won, "Surface plasmons: optical antennas for sensing," Nat. Photonics **1**, 442 (2007).
24. E. J. Smythe, E. Cubukcu and F. Capasso, "Optical properties of surface plasmon resonances of coupled metallic nanorods," Opt. Express **15**(12), 7439-7447 (2013).
25. D. Ramaccia, F. Bilotti, A. Toscano and A. Massaro, "Efficient and wideband horn nanoantenna," Opt. Lett. **36**(10), 1743–1745 (2011).
26. L. Yousefi and A. C. Foster, "Waveguide-fed optical hybrid plasmonic patch nano-antenna," Opt. Express **20**(16), 18326-18335 (2012).
27. Y. Yang, D. Zhao, H. Gong, Q. Li, and M. Qiu, "Plasmonic sectoral horn nanoantennas," Opt. Lett. **39**(11), 3204–3207 (2014).
28. M. Saad-Bin-Alam, I. Khalil, A. Rahman and A. M. Chowdhury, "Hybrid plasmonic waveguide fed broadband nanoantenna for nanophotonic applications," IEEE Photon. Technol. Lett. **27**(10), 1092–1095 (2015).
29. K. J. A. Ooi, P. Bai, M. X. Gu and L. K. Ang, "Design of a monopole-antenna-based resonant nanocavity for detection of optical power from hybrid plasmonic waveguides," Opt. Express **19**(18), 17075–17085 (2011).
30. Z. Pan and J. Guo, "Enhanced optical absorption and electric field resonance in diablo metal bar optical antennas," Opt. Express **21**(26), 32491-32500 (2013).
31. H. Guo, T. P. Meyrath, T. Zentgraf, N. Liu, L. Fu, H. Schweizer, and H. Giessen, "Optical resonances of bowtie slot antennas and their geometry and material dependence," Opt. Express **16**(11), 7756-7766 (2008).
32. T. H. Timiniau, F. D. Stefani and N. F. van Hulst, "Enhanced directional excitation and emission of single emitters by a nano-optical Yagi-Uda antenna," Opt. Express **16**(14), 10858–10866 (2008).
33. P. B. Johnson, and R. W. Christy, "Optical constants of noble metals," Phys. Rev. B **6**(12), 4370–4379 (1972).
34. P. J. Gibson, "The Vivaldi aerial," Proceedings of the 9th European Microwave Conference (EuMC), (IEEE 1979), pp. 101–105.
35. J. Shin and D. H. Schaubert, "A parameter study of stripline-fed Vivaldi notch-antenna arrays," IEEE Trans. Antennas Propag. **47**(5), 879–886 (1999).
36. Z. Iluz and A. Boag, "Dual-Vivaldi wideband nanoantenna with high radiation efficiency over the infrared frequency band," Opt. Lett. **36**(15), 2273–2775 (2011).
37. I. S. Maksymov, I. Staude, A. E. Miroshnichenko and Y. S. Kivshar, "Optical Yagi-Uda nanoantennas," Nanophotonics **1**(1), 65–81 (2012).
38. COMSOL Multiphysics, http://www.comsol.com/
39. Lumerical Solutions, Inc. http://www.lumerical.com/tcad-products/fdtd/
40. M. C. Greenberg, L. Virga and C. L. Hammond, "Performance characteristics of the dual exponentially tapered slot antenna for wireless communication application," IEEE Trans. Veh. Technol. **52**(2), 305–310 (2003).
41. J.D. Kraus, *Antennas, 2nd Ed.* (McGraw-Hill, 1988).
42. B. Ciftcioglu, R. Berman, S. Wang, J. Hu, I. Savidis, M. Jain, D. Moore, M. Huang, E. G. Friedman, G. Wicks and H. Wu, "3-D integrated heterogeneous intra-chip free-space optical interconnect," Opt. Express **20**(4), 4331–4345 (2012).
43. A. Taflove, *Computational Electromagnetics: The Finite-Difference Time-Domain Method* (Artech House, 2005).

1. Introduction

Chip Multiprocessors (CMP) exploiting parallel computation capabilities are the state of the art solution to face the constant need of increasing computing system efficiency. A CMP replicates different processing cores on the same die, working in parallel on isolated CPU operations, and interconnected to share resources. In these configurations, as the number of computational units increases, efficient interconnection among the processors is becoming a major challenge. To this purpose, traditional bus architectures have been replaced with Network on Chip (NoC) topologies [1]. In more aggressive approaches, optical interconnections on chip (ONoC) are

Optics EXPRESS

proposed [2–4]. The introduction of ONoC can be disruptive in term of bandwidth, latency and power consumption [5]. Major drawbacks, in this case, are represented respectively by footprint increasing and layout complexity, with consequent difficult implementation of the routing algorithms, and by the high signal loss due to inevitable multiple waveguide crossings, which worsen the overall power budget [6]- [8]. For these reasons, wireless connections (WiNoC) have been investigated as a complementary solution to link distant cores [9–11]. In these approaches, the operation frequency ranges from tens (millimeter waves) to hundreds of THz (near-infrared). A survey of WiNoC propagation and the issues involved in channel modeling have been addressed in [12].

The use of on chip wireless connections through optical signals (OWiNoC) allows combining the advantages of both ONoC and WiNoC approaches, without requiring frequency converters and transceivers. With this technique, in fact, optical signals could be either routed through waveguides or wireless links, thus avoiding integration of electronic devices for electro-optical conversions, reducing complexity and energy costs. The elimination of electro-optical conversion has also the potential to guarantee bitrate transparency and distance independence of the photonic links. Optical wireless broadcasting links have been initially suggested in [13], where better performance with respect to regular plasmonic waveguides has also been demonstrated. The design of efficient broadband wireless nanolinks and networks is presented in [14], where power transfer using on-chip integrated plasmonic antennas is compared to a direct waveguide-based interconnect. In this work, horn nanoantennas with a large footprint are proposed, being the metal deposited on a wide area on the chip. In [15], a short-distance in-plane wireless communication system via nanoscale plasmonic antennas has been experimentally demonstrated. Here, the authors investigate the use of dipoles, which are known to have a small directivity. For optical wireless communications, antennas with high efficiency are key components whose optimization is essential to cope with problems related to the attenuation determined by light propagation in an unbounded medium. In fact, at optical frequencies the distance between processors allocated on the same chip, though not very large in absolute terms, is significant if considered with respect to the used wavelengths. In [16] authors show how the use of impedance-matched and directive nanoantennas enhance the capability of an optical wireless link even with respect to regular plasmonic waveguide connects which, by suffering from metal absorption, are outperformed by wireless connections for distances larger than 8 μm.

Optical antennas convert freely propagating optical radiation into localized energy, and vice versa [17]. They allow manipulation of the light at the nanoscale, while enabling controlling of the far field emission. Advances in fabrication technologies have resulted in a strong increase of the use of these devices [18]. Optical antennas are having a disruptive impact on a variety of fields such as microscopy [19], nonlinear optics [20], photoemission and photodetection [21,22], sensing [23] and spectroscopy [24]. Examples of nanoantennas for optical interconnections are illustrated in [25–28]. These antennas have been inspired from different designs of microwave radiators and optimized both to match the impedance and to provide high directivity in the optical telecommunication wavelength range. Some antennas are based on simple designs such as Dipole or Bow-Tie [29–31], but also more complex implementations such as Yagi-Uda have been proposed [32]. Hybrid solutions using plasmonic antennas with waveguide feeding [26–28] are better suited for OWiNoC applications, for easy integration between wired and wireless connections.

In this paper, we propose the design of a Vivaldi plasmonic antenna for on-chip optical communications and numerically investigate the performance of an optical wireless link based on this suitably designed antenna. The Vivaldi antenna [34], often used in the microwave range when high-gain and relatively large bandwidth are required [35], is a good candidate for optical wireless communications. In fact, by suitably tailoring the antenna geometry, it is possible to

Optics EXPRESS

obtain good performance also at optical frequencies [36]. This antenna has been chosen among the possible ones as it provides a simple geometry, a small side extension, a high gain and a large operating bandwidth. Nonetheless, the design criteria and the propagation analysis proposed in this work can be easily applied to other aperture antenna geometries, such as horn antennas.

A large bandwidth is required in OWiNoCs, to allow wireless communication of the entire WDM spectrum propagating in the optical wired links and to guarantee the high capacity needed by intra-chip communications. High gain is desirable to limit the transmitted power and, therefore, to reduce the overall power consumption. Other proposed optical nanoantennas do not provide such a high gain (see for example [26] and [28]) or bandwidth (such as the dipole or Yagi-Uda: see [37] for discussion on this point). Moreover, excitation through silicon waveguides is not straightforward [32]. In the investigated design, the Vivaldi is obtained by properly shaping a slotted microstrip deposited above a silica substrate. The antenna has been tailored for high gain and efficient feeding, to significantly enhance port-to-port communications. The high gain maximizes the power budget of the link. Moreover, it minimizes possible interference with other wireless optical connections and undesired coupling with the circuitry, thus allowing an increase in circuit integration. Transmitting and receiving sections have been designed to allow a direct and efficient coupling between the antennas and the optical waveguides used for signal distribution among the processors.

The paper is organized as follows: in the next section, after a short description of the proposed antenna, the transition between the silicon waveguide and the plasmonic structure is optimized. Then, design and maximization of the performance of the optical antenna in the C-band (1530 – 1565 *nm*) are addressed. Finally, results relevant to the simulation of a point-to-point wireless link are presented and discussed. The gain of the antenna obtained through near-to-far field transformation is compared with the one determined through the direct full-wave simulation of a wireless connection.

2. Design and optimization of the feeding section of the optical antenna

The geometry of the proposed structure is sketched in Fig. 1. The device consists of a silicon waveguide (*Si*, refractive index $n = 3.470$) exciting the plasmonic antenna. The two structures are immersed in silica (SiO_2, $n = 1.444$).

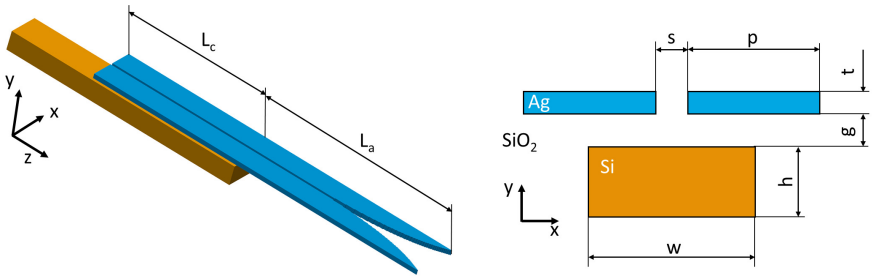

Fig. 1. Sketch of the optical antenna: 3D view (left); lateral view (right). The ochre geometry represents the silicon waveguide, whereas the light-blue one is the plasmonic structure. The silicon waveguide has dimensions $w \times h$. The gap between the photonic wire and the plasmonic structure is g, while s is the width of the slot between the two arms of the plasmonic waveguide. The thickness of the metallic strip is t and the width of each arm is p. L_c is the length of the coupling section, whereas L_a is the length of the antenna.

In this geometry, three sections can be identified: the dielectric waveguide, the coupler and the Vivaldi antenna. The aim of the coupling section is to allow an efficient transfer of the photons from the silicon wire to the plasmonic waveguide (in the transmitting section) and vice versa

Optics EXPRESS

(at the receiver). The plasmonic waveguide is then used to excite the antenna (or to receive the photons collected by the antenna). The antenna is obtained by properly shaping a slotted microstrip deposited above the silica substrate. In this work, the material used for the plasmonic waveguide is Silver, but other metals such as Aluminum or Gold could also be considered: what is really important for the fabrication of the structure is the compatibility of the used materials with standard CMOS processing techniques, which guarantees the compatibility of the process for both the electronic and the optic layers. In our simulations to describe the complex permittivity of the Silver we used a dispersive model with Johnson and Christy parameters [33]. In the investigated configuration (see Fig. 1), the antenna is fed through a *Si* photonic wire and positioned at the end of the silicon waveguide, to minimize the influence of the silicon wire on its radiation diagram.

In order to design the transition between the silicon and the plasmonic slotted waveguide, the results of the Coupled Mode Theory (CMT) and of the normal mode analysis have been exploited. Although the CMT is not rigorous when strongly coupled waveguides are considered, it can be used to achieve the geometrical design with negligible computational effort, provided further verifications and optimizations of the chosen configuration with fullwave simulations. According to the CMT, the overall structure can be considered as the superposition of two waveguides, i.e. the *Si* and the plasmonic slotted waveguide. To maximize the power transfer, the synchronism condition between waveguide modes must be verified (i.e. the detuning factor $\delta = \beta_2 - \beta_1 = 0$, with β_1 and β_2 being the propagation constants of the modes of the two isolated waveguides we require to couple). This means that the effective refractive indices (n_{eff}) of the two waveguide modes must be equal. This condition can be verified by properly tailoring the geometrical parameters of the coupler. It is worth underlying that, in order to apply a very simple design procedure, losses have not been included in the Coupled Mode Theory (CMT). Therefore, the synchronism condition and the coupling length have been calculated considering only the real part of the effective refractive indices.

For the design of the coupling section, the Finite Element Method (FEM) [38] has been exploited including (structure) losses. The synchronization of the fundamental TE modes of the two structures has been obtained by optimizing the widths of the silicon (w) and of the plasmonic (p) waveguides. The heights have not been used as geometrical parameters for tailoring, since each value is settled by other constraints. For example, for the silicon waveguide we have chosen $h = 220\ nm$, to guarantee the compatibility with other photonic wires used for signal distribution inside the chip (this is the standard waveguide height for waveguides in SOI technology). The thickness of the plasmonic structure, on the contrary, has been adjusted by taking into account possible technological constraints. To avoid complications in the fabrication process, in fact, a thickness $t = 50\ nm$ has been considered. The design has been optimized for $\lambda = 1.55\ \mu m$, which is the central wavelength of the WDM spectrum we are supposing to use for signal distribution.

Figure 2(a) relates the effective refractive indices of the fundamental TE mode of both the silicon and the photonic waveguides to the pertinent waveguide width (w for the silicon wire, p for the plasmonic structure). The black dashed curve refers to the *Si* structure, whereas colored solid curves are for the plasmonic waveguide: plots for different values of the slot width s are shown (from $s = 20\ nm$ (blue curve, the rightmost one in the plot) to $s = 70\ nm$ (yellow curve, the leftmost one in the plot)). For an assigned value of n_{eff}, waveguide widths are chosen through intersections with the corresponding curves. For example if $n_{eff} = 2.4$ (vertical dash-dotted line), $w = 480\ nm$ (which is the width of standard waveguides in SOI technology) and $p = 80\ nm$, for a plasmonic waveguide with a slot $s = 30\ nm$ (green curve in Fig. 2(a)). The solution is clearly not unique: in fact, even once selected the slot width s, different combinations of n_{eff}, w and p are allowed. Therefore, the choice should be made by considering other aspects such as, for example, the difficulty of the fabrication process, the amount of losses, the footprint,

Optics EXPRESS

etc.

In order to operate a unique selection of the geometrical parameters, we calculated the coupling length L_c for the different couples of width values (w and p) by computing the supermodes (i.e. the normal modes of the overall structure formed by the silicon and the plasmonic waveguides) of the two-waveguides structure. According to the normal mode analysis, once verified the synchronism condition, the coupling length L_c can be calculated as:

$$L_c = \frac{\lambda}{2\,(n_{c1} - n_{c2})} \tag{1}$$

where n_{c1} and n_{c2} are the effective refractive indices of the first two normal modes of the overall structure. In our simulations, we used a vertical gap between the two waveguides $g = 80\ nm$. Moreover, we focused our attention on a plasmonic waveguide with a slot $s = 30\ nm$, which is compatible with current fabrication technology. The coupling length as a function of the effective refractive index of the two waveguides is reported in Fig. 2(b). For a $n_{eff} = 2.4$, the coupling length results $L_c = 5.2\ \mu m$ (dash-dotted line in Fig. 2(b)). A shorter coupling length can be obtained by operating with smaller values of the effective refractive index. By choosing for example $n_{eff} = 2.17$ (dotted vertical line in Fig. 2(b)), $L_c = 1.63\ \mu m$, which is much shorter than the coupling length previously determined. This last configuration has been preferred for two reasons: (i) being the plasmonic waveguide shorter, losses in the metal are minimized and better efficiency for the antenna could be obtained; (ii) the width of the plasmonic waveguide is not critical for the performance of the coupler. In fact, the curve relating the effective refractive index to the width p is vertical, in practice (see the green plot in Fig. 2(a)), meaning that a large tolerance in the choice of p is permitted (by changing p, the corresponding n_{eff} is practically constant). This condition definitely eases the fabrication process, where the control of the geometry could be difficult. With this value of the effective refractive index, by considering in Fig. 2(a) the intersection of the dotted vertical line with the green curve ($s = 30\ nm$) of the plasmonic waveguide, the width p results $p = 270\ nm$. For the silicon waveguide, the intersection of the dotted vertical line with the dashed black curve gives $w = 380\ nm$. The final configuration of the geometry of the coupler is therefore: $w = 380\ nm$, $s = 30\ nm$, $p = 270\ nm$ and $L_c = 1.63\ \mu m$.

For completeness, we have also evaluated the bandwidth of the coupler. To this purpose, S parameters have been computed in the $1.5\ \mu m - 1.6\ \mu m$ wavelength range. The input port has been defined in the cross section of the silicon waveguide, before the region where the two waveguides are superimposed. A cross section of the the plasmonic slotted waveguide has been considered as the output port of the device. In these simulations, the antenna has not been included in the scenario. The inset in Fig. 2(b) shows the reflection ($|S_{11}|$, black dashed plot) coefficient at the input port and the transmission coefficient ($|S_{21}|$, red solid curve) between the two ports. The power transfer is good in the whole wavelength range ($|S_{21}| > -1\ dB$) and the reflection coefficient is always limited ($|S_{11}| < -18\ dB$).

3. Optimization of the Vivaldi antenna

The Vivaldi antenna has been designed through simulations performed by using Lumerical FDTD [39]. The geometrical parameters involved in the optimization procedures are the antenna length L_a and the exponential taper profile, adjusted via the opening rate coefficient R [40]. R influences the shape of the antenna aperture: larger values correspond to smoother transitions between the gap and the antenna termination, whereas smaller values give almost straight transitions, making the Vivaldi more similar to a horn antenna. Except for these two parameters, the antenna geometry (the width p of the two metallic strip, their thickness t and the width s of the slot) depends on the dimensions of the plasmonic waveguide used in the feeding section. In

Optics EXPRESS

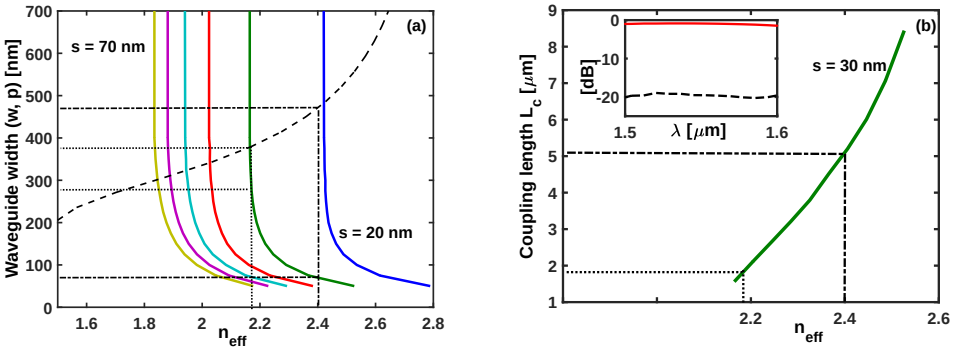

Fig. 2. On the left: Plot of the curves relating the effective refractive index n_{eff} of the fundamental TE mode of the isolated waveguides to the waveguide width (w or p), respectively for the photonic wire (black dashed curve) and for the plasmonic waveguide (colored solid curves). For the plasmonic waveguide, curves are plotted as a function of the slot width s from $s = 20\ nm$ (blue curve, the rightmost one in the plot) to $s = 70\ nm$ (yellow curve, the leftmost one in the plot). In these simulations, $\lambda = 1.55\ \mu m$. On the right: Coupling distance L_c as a function of the effective refractive index n_{eff} for a coupler with a $s = 30\ nm$ slotted plasmonic waveguide. In these simulations, $\lambda = 1.55\ \mu m$. The inset of the right figure shows the S parameters (red solid curve for $|S_{21}|$ and black dashed curve for $|S_{11}|$) of the coupler in the $1.5\ \mu m - 1.6\ \mu m$ wavelength range.

fact, the Vivaldi is built as an extension of this structure, to ease the fabrication of the device. As discussed in the introduction, the quantities to be optimized for the applications considered in this work are the gain and the bandwidth.

The importance of having a broadband device is straightforward: a broadband antenna allows efficient irradiation of all the carriers used for the communications inside the chip, avoiding any time and energy consuming processing to aggregate different channels. To better appreciate the fundamental role of the gain on the link performance, the attenuation introduced by free space propagation as a function of the distance should be considered. When the connection takes place in a homogeneous medium and between two antennas in the far-field region, both matched in impedance and polarization, the link power budget can be obtained through the well known *Friis* transmission equation [41]:

$$P_r = P_t + G_r + G_t + 20\ log_{10}\left(\frac{\lambda/n}{4\pi d}\right), \tag{2}$$

where P_r and P_t are respectively the received and the transmitted powers (in dBm), G_r and G_t are the antenna gains (in dB), λ is the wavelength of the electromagnetic wave used for the connection, n is the refractive index of the medium and d is the distance between the two antennas. In this equation, the last term describes the loss in signal strength of an electromagnetic wave that would result from a line-of-sight path through free space. It is usually known as Free-Space Path Loss (FSPL) and expressed in dB as $A_0 = -20\ log_{10}\ (\lambda/(4\pi dn))$. As one can notice, the power drops with the square value of the distance normalized with respect to the wavelength of the used carrier. The *Friis* transmission equation is commonly used in telecommunications engineering when linking two antennas under idealized conditions, such as infinite and homogeneous propagation medium. This condition could obviously not be verified when the connection takes place inside a chip, and it is only used here for a rough estimation of both the attenuation and the antenna parameters needed to guarantee the possibility of an

Optics EXPRESS

efficient point-to-point connection.

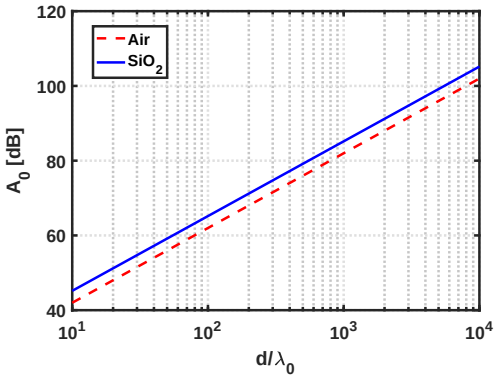

Fig. 3. Free-Space Path Loss A_0 (in dB) of a wireless connection as a function of the distance (normalized with respect to the wavelength) between the transmitting and the receiving antennas for a link in air (blue solid curve) and on a homogeneous SiO_2 (red dashed curve), respectively.

Figure 3 shows the attenuation of a wireless connection as a function of the distance (normalized with respect to the wavelength): the attenuation grows with the distance, and is larger when the wave propagates on a medium denser than the air. For example, if an optical link of 50 μm at the wavelength $\lambda = 1.55$ μm is considered, the FSPL is $A_0 = 52.16$ dB in air ($n = 1$), and $A_0 = 55.35$ dB in silica, where the refractive index is larger ($n = 1.444$). These values of the attenuation become respectively $A_0 = 58.18$ dB in air and $A_0 = 61.37$ dB in silica for a link 100 μm long, but they grow to $A_0 = 98.18$ dB in air and $A_0 = 101.37$ dB in silica for a wireless connection of 1 cm, which is the distance among the cores that should be considered for intra-chip optical wireless connections [42]. To cope with the Free-Space Path Loss, antennas with high gain are therefore mandatory in OWiNoC applications.

To investigate the performance of the Vivaldi antenna, the radiation pattern and the directivity as a function of the wavelength have been considered first. Directivity and radiation patterns have been obtained by performing standard near-to-far field projections of the fields recorded, for different wavelengths (and therefore once applied Fourier transformations on time-domain FDTD field values), on a closed box surrounding the antenna [43]. The structure has been excited, in the 1.5 μm – 1.6 μm wavelength interval, with the fundamental TE mode of the silicon photonic wire. The results obtained for a Vivaldi with length $L_a = 2.5$ μm and opening rate $R = 3.0$ μm^{-1} are illustrated in Fig. 4(a). In this figure, the directivity is plotted with respect to the wavelength, and ranges from a minimum of 9.0 dB (for $\lambda = 1.500$ μm) to a maximum of 11.1 dB (for $\lambda = 1.554$ μm). In the considered wavelength range, the reflection coefficient at the input port (the feeding section of the silicon waveguide exciting the antenna) $|S_{11}|^2$ is small and slowly varying: in fact, it spans between -8.0 dB and -11 dB. The proposed antenna, from the point of view of both directivity and impedance matching at the input port, has therefore a sufficient bandwidth to efficiently radiate WDM signals in the 1.55 μm telecommunication band.

The radiation patterns of the antenna in the horizontal (xz) plane are also plotted in Fig. 4(b), respectively for $\lambda = 1.5$ μm (top plot), $\lambda = 1.55$ μm (central plot) and $\lambda = 1.6$ μm (bottom plot). The antenna maintains its main lobe always in the same direction (along its axis), and can therefore be exploited to operate in a point-to-point configuration. These properties show that the proposed antenna is well suited to be used in OWiNoC. As the Vivaldi antenna radiates a linearly polarized field with the main E-field component on the xz plane, where the antenna has

Optics EXPRESS

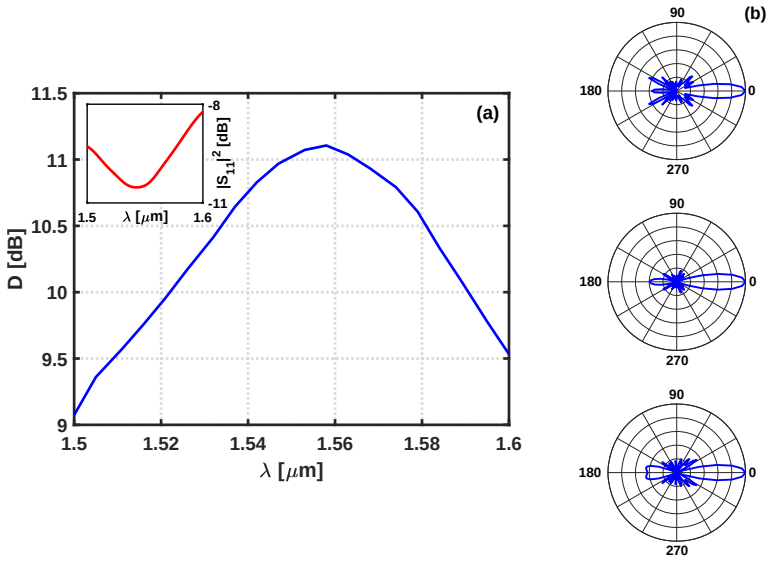

Fig. 4. On the left: directivity of the Vivaldi antenna for $L_a = 2.5\ \mu m$ and $R = 3.0\ \mu m^{-1}$ as a function of the wavelength in the $1.5\ \mu m - 1.6\ \mu m$ wavelength range. The inset shows the reflection coefficient ($|S_{11}|^2$) at the input port in the same wavelength interval. On the right: radiation patterns of the Vivaldi Antenna on the horizontal (**E**) plane for $\lambda = 1.5\ \mu m$ (top plot), $\lambda = 1.55\ \mu m$ (central plot) and $\lambda = 1.6\ \mu m$ (bottom plot).

also the direction of maximum radiation, we will refer to this as the **E** plane of the antenna, as usual in antenna theory. Moreover, the *yz* plane contains the main H-field component and the direction of maximum radiation. Therefore, we will refer to this plane as the **H** plane.

The optimization of the Vivaldi antenna has been performed by simulating the structure of Fig. 1 for different values of the antenna length L_a first, and then by changing the opening rate R. We performed the optimization with respect to the antenna gain G, which is related to the directivity D through the antenna efficiency. The gain is better suited to evaluate the performance of an antenna on a link. In fact, it enters directly in the formula of the power budget (see Eq. (2)) and represents a figure of merit which takes into account both the directional properties of the antenna and its capabilities to irradiate the power supplied at the input port. The antenna efficiency is calculated by taking into account the reflection coefficient at the input port and the power dissipated on the antenna due to the conductivity of the metal [14]. We focused our investigations at the central wavelength ($\lambda = 1.55\ \mu m$), and computed the gain as a function of L_a when $R = 3.0\ \mu m^{-1}$. Results are shown in Fig. 5(a). The directivity of the antenna (red-dashed curve, right axis) has a maximum of 11.8 *dB* for $L_a = 4.25\ \mu m$. However, due to the absorption in the metal, for this configuration the gain is not maximized ($G = 9.3\ dB$): a better performance is obtained for $L_a = 1.75\ \mu m$, where $G = 9.8\ dB$ (the antenna is shorter in this configuration, and therefore losses in the metal are weaker), although the directivity is slightly reduced to $D = 11.5\ dB$. From our simulations we observed a periodic behavior of the directivity as a function of the length L_a, with maxima corresponding to resonances of the structure. These maxima have higher values of the directivity for longer antennas, but due to losses in the metal the gain does not follow this trend, and the best performance are obtained for a small value of L_a. In Fig. 5(b) the radiation patterns of the investigated structure ($L_a = 1.75\ \mu m$, $R = 3.0\ \mu m^{-1}$) are reported for three different values of the wavelength. The top plot is for $\lambda = 1.50\ \mu m$; the central plot is for $\lambda = 1.55\ \mu m$ whereas the bottom one is for

Optics EXPRESS

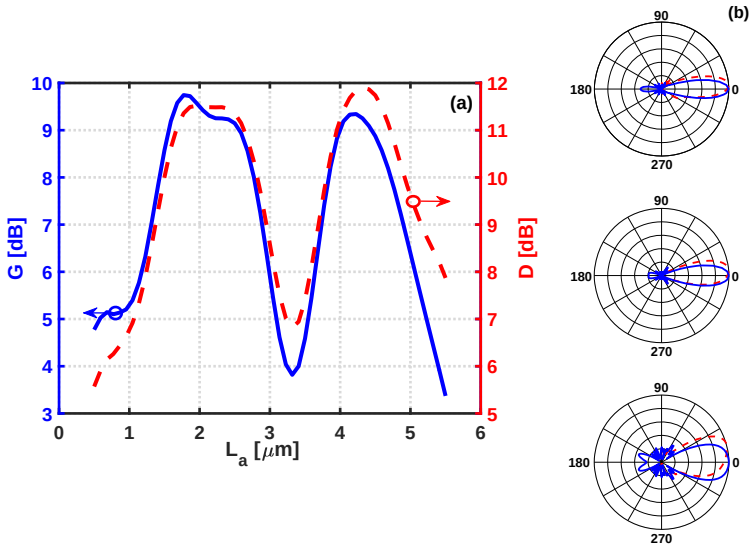

Fig. 5. On the left: directivity (red dashed curve, right axis) and gain (blue solid curve, left axis) of the Vivaldi antenna as a function of L_a. In these computations, $R = 3.0\ \mu m^{-1}$ and $\lambda = 1.55\ \mu m$. On the right: radiation patterns for $\lambda = 1.50\ \mu m$ (top plot), for $\lambda = 1.55\ \mu m$ (central plot) and for $\lambda = 1.60\ \mu m$ (bottom plot). The blue solid curves show the radiation patterns in the horizontal (**E**) plane, whereas the red dashed curves refer to the vertical (**H**) one. For these simulations, antenna parameters are $L_a = 1.75\ \mu m$, $R = 3.0\ \mu m^{-1}$.

$\lambda = 1.60\ \mu m$. In all the plots, the blue solid curves are the radiation patterns in the **E** plane, while the red dashed lines are the radiation patterns in the **H** one. As it can be noticed, the maximum of the radiation is along the axis of the antenna (z axis). In the vertical **H** plane, the antenna radiates with a small tilt (less than $10.0°$ for $\lambda = 1.55\ \mu m$). This is due to the presence of the silicon feeding waveguide, which perturbs the vertical symmetry of the structure and causes a reduction of the gain of about $0.15\ dB$ on the horizontal plane. To limit this undesired tilt, the Vivaldi antenna was shifted with respect to the photonic wire, of an amount determined by the length L_a optimized for a maximum of the gain G.

The effects of the opening rate R on both the gain and the directivity are reported in Fig. 6(a). The directivity has a maximum of $D = 11.8\ dB$ (red dashed curve, right axis) for $R = 3.5\ \mu m^{-1}$. For this configuration, also the gain is maximum (blue solid curve, left axis in the same figure) and holds $G = 9.95\ dB$. The parameters of the optimized Vivaldi antenna are therefore $L_a = 1.75\ \mu m$ and $R = 3.5\ \mu m^{-1}$. Figure 6(b) shows the gain as a function of the wavelength. In the wavelength range of the C-band ($1530 - 1565\ nm$), the gain spans from the minimum value of $G = 9.20\ dB$ to the maximum value of $G = 9.95\ dB$, and is bigger than the one of the similar antennas investigated in [14] and [28]. The inset of the same figure shows that the reflection coefficient at the feeding port is still small and slowly variable, being always limited to $|S_{11}|^2 < -8\ dB$; this confirms that the proposed antenna can be efficiently used for OWinOC applications. The total antenna efficiency, evaluated through the ratio between the gain and the directivity, is $\eta_t = 0.65$. This value includes the coupling efficiency η_c and the radiation efficiency η_r, being $\eta_t = \eta_c \cdot \eta_r$. The radiation efficiency accounts for the losses inside the antenna, that could be in both the dielectric (dielectric losses) and the metal (conduction losses). The coupling efficiency takes instead into account the impedance mismatch at the input of the antenna, and it is related to the reflection coefficient $|S_{11}|$. As $|S_{11}|^2 = -10.5\ dB$, $\eta_c = 1 - |S_{11}|^2 = 0.91$. It follows that

Optics EXPRESS

$\eta_r = \eta_t/\eta_c = 0.71$. This means that about the 30% of the input power is dissipated into the plasmonic structure.

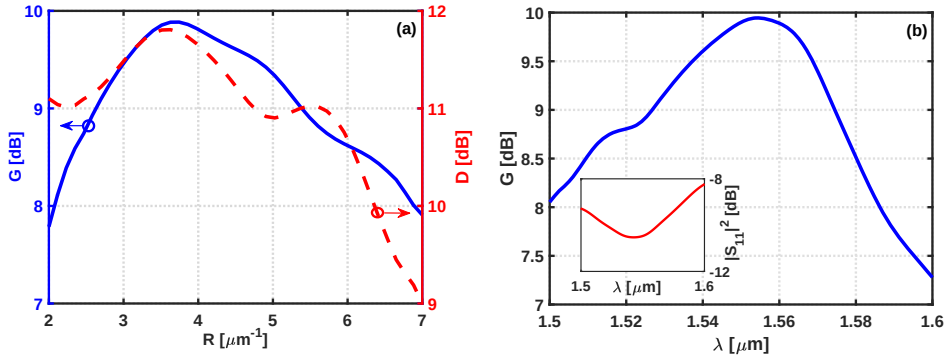

Fig. 6. On the left: directivity (red dashed curve, right axis) and gain (blue solid curve, left axis) of the Vivaldi antenna as a function of R and for $\lambda = 1.55\ \mu m$. In these computations, the length of the antenna is $L_a = 1.75\ \mu m$, which is the optimized value obtained previously. On the right: gain of the optimized antenna ($L_a = 1.75\ \mu m$ and $R = 3.5\ \mu m^{-1}$) as a function of the wavelength. The inset shows the reflection coefficient $|S_{11}|^2$ in the $1.5\ \mu m - 1.6\ \mu m$ wavelength interval.

For these simulations we used a variable-conformal mesh, with a minimum step size of 7 *nm*. The computational domain extended for 11 μm along the propagation direction (z axis), and for 2.5 μm on both the directions of the transverse (xy) plane. We used stretched coordinate Perfectly Matched Layers (PML) to absorb the outgoing fields at the edges of the simulated region. Each simulation required about one hour running in parallel on 10 processors (Intel Xeon E5620) to compute all the field components in the near field region. Near-to-far field projections are computed once finished the FDTD simulation. Convergence tests have shown that, by reducing the mesh size to a minimum step size of about 4.5 *nm*, the calculated value of the directivity changed of less than 2.5%, while the computation time increased to more than two hours.

4. Performance of the optical wireless link

Finally, the performance of a wireless link has been investigated by simulating a connection between two Vivaldi antennas coupled with their silicon waveguides and positioned in the far field region, so that FDTD simulation results can be compared with the ones obtained via the *Friis* formula of Eq. (2). To this purpose, the transmitting *TX* and receiving *RX* antennas have been positioned 50 μm apart, a distance that verifies the hypothesis of the far-field region, embedded in homogeneous silica. A sketch of the wireless link is illustrated in Fig. 7. In this picture, the input and output ports of the link have been highlighted. These ports are defined on the Silicon waveguides respectively at the transmitter (TX) and at the receiver (RX), and allow to compute, through evaluation of the power fluxes, the power P_t supplied to the transmitting antenna and the power P_r collected by the receiver. In this way, the power budget of the link can be directly calculated from the FDTD results.

As previously pointed out, the approach based on the *Friis* transmission equation represents an idealistic propagation condition used here to test the performance of the proposed antennas. In more realistic conditions, for OWiNoC applications the propagation will be strongly influenced by the discontinuities introduced by the layered structure of the chip and by the presence of other optical devices in the propagation medium. Investigations on the effects of

Optics EXPRESS

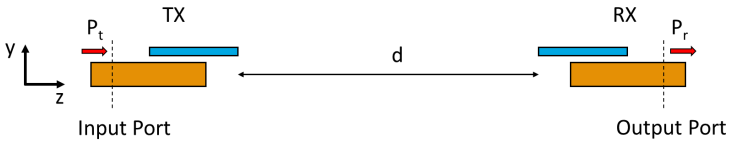

Fig. 7. Sketch of the wireless optical link with definition of the input and output ports on the silicon waveguides respectively at the transmitter and the receiver. P_t is the input power on the *Si* waveguide exciting the *TX* antenna, whereas P_r is the output power collected by the waveguide at the *RX* section. d is the length of the optical wireless link.

these discontinuities will be the central topic of a further paper.

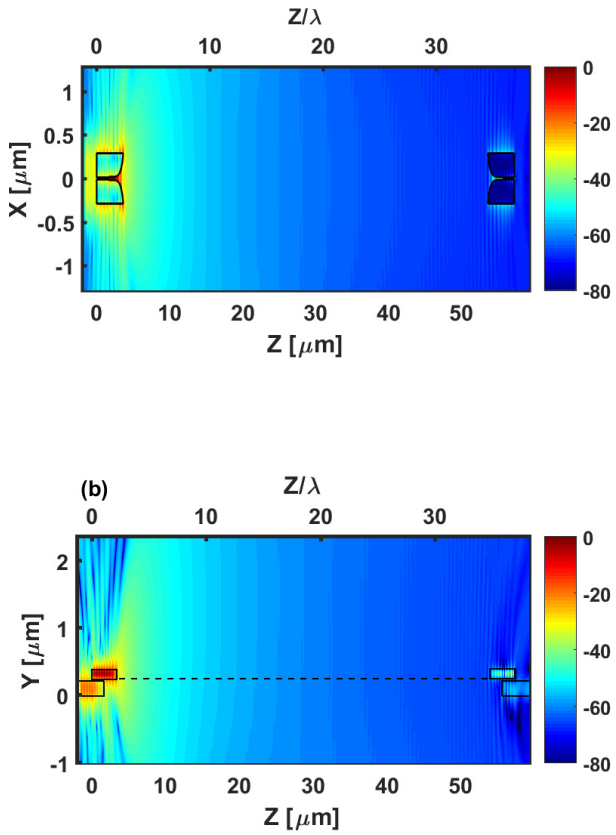

Fig. 8. Pattern of the electric field $|E|^2$ (logarithmic scale) on the horizontal (top plot) and vertical (bottom plot) planes for an optical link between two antennas embedded on silica and positioned 50 μm apart. The wavelength is $\lambda = 1.55$ μm. Axes are not in scale, to ease visualization. The top axis in both plots shows the Z coordinate normalized with respect to the propagation wavelength.

Figure 8 shows the patterns of the electric field intensity $|E|^2$ for an optical link between

Optics EXPRESS

two antennas embedded in silica and positioned 50 μm apart. The top plot (Fig. 8(a)) refers to a horizontal xz plane passing at the center of the metal layer. The bottom plot (Fig. 8(b)) is instead for a vertical yz plane at the center of the computational domain. The wavelength is $\lambda = 1.55\ \mu m$. From this picture it is possible to observe the decay of the field intensity with the distance, but also the positive consequences of the directivity of the antenna. The power collected at the output waveguide is also evident. This confirms the beneficial effect of both the transmitting and the receiving antennas. The former, which is able to control the far-field emission through manipulation of the field at the nanoscale. The latter which collects photons from the free space and transfers the received power toward the output port.

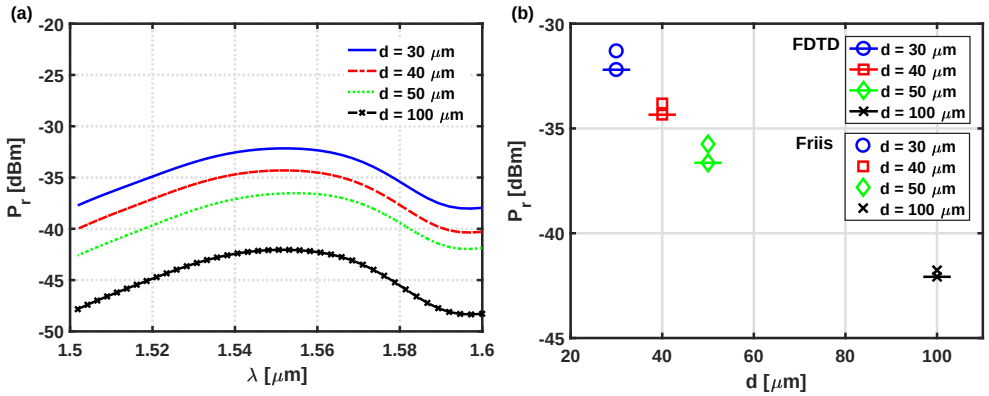

Fig. 9. On the left: plots of the received power (in dBm) at the output port of the link for different connection lengths d in the 1.5 μm – 1.6 μm wavelength interval. On the right: comparisons among the received powers obtained, for different connection lengths d, by simulating with FDTD the whole link and through the *Friis* equation with the values of the antenna gain obtained in the previous section. In these simulations, $\lambda = 1.55\ \mu m$.

The received power at the output section of the link as a function of the wavelength is plotted in Fig. 9(a). Different link distances have been investigated. Being the values normalized to an input power of $P_t = 0\ dBm$, the power P_r measured at the output port is directly the power budget of each connection. As expected, the maximum efficiency is obtained for $\lambda = 1.55\ \mu m$, where the TX and RX antennas are optimized for the higher gain. For this wavelength, by considering that for $d = 50\ \mu m$ the free-space path loss $A_0 = -55.35\ dB$, the received power is $P_r = -36.50\ dBm$, and the fact that the two antennas are identical, the estimated gain from the *Friis* equation is $G_F = 0.5\ (P_r - P_t - A_0) = 9.425\ dB$, in good agreement with the values previously determined. In fact, from FDTD simulations of the Vivaldi antenna with near-to-far field projections we obtained a gain $G = 9.95\ dB$. However, due to the tilt of the radiation pattern in the vertical plane (see the red dashed curve on the central plot of Fig. 5(b), where the radiation patterns for $\lambda = 1.55\ \mu m$ are illustrated, a reduction of 0.15 dB is expected. Therefore, $G = 9.8\ dB$ and the relative error for the evaluation of the gain with the two approaches $(G - G_F)/G \cdot 100$ is of about 3.8%. When $d = 100\ \mu m$, the gain from the full-wave simulation of the link is a bit higher ($G_F = 9.67\ dB$); in this case, the relative error is smaller than 1.3%. In all our simulations, the relative error for the gain was always smaller than 3.9%. We think that this error is determined by the differences in the mesh used in FDTD simulations when computational domains with different lengths are represented. Figure 9(b) compares the received powers P_r obtained via FDTD simulation of the whole link and through the use of the *Friis* equation with the value of the antenna gain obtained with the simulation of the single antenna. Different connection lengths d have been considered. In these simulations, $\lambda = 1.55\ \mu m$. As it can be noticed, the differences between the results obtained with the two approaches are very small.

Optics EXPRESS

The maximum error in the received power is always smaller than 3.0%.

As for the computation of the antenna parameters, for these simulations we used a variable-conformal mesh, with a minimum step size of 7 *nm*. For the case relevant to a link distance of 50 μm, the computational domain extended for 62 μm along the propagation direction (z axis), and for 2.5 μm on both the directions of the transverse (xy) plane. We tested the accuracy of the results by reducing the mesh to a minimum step size of 5 *nm*, and obtained a modification in the received power P_r of less than 6.0%. As the computation time increased from 6 to 16 hours running the simulation in parallel on 12 processors, we decided to keep the mesh resolution previously used for the design of the Vivaldi antenna.

5. Conclusion

In this paper we have proposed a hybrid optical plasmonic Vivaldi antenna for Optical Wireles Network on Chip applications operating in the standard C (1530 – 1565 *nm*) telecommunication band. The antenna is fed by a silicon waveguide and is compatible with standard SOI technology. The design reports a gain of about 10 *dB* and a bandwidth which largely covers all the spectrum of the C band. The antenna maintains its main lobe always along its axis, and can therefore be exploited to operate in a point-to-point connection for inter- or intra-chip optical communications. Direct port-to-port short links have also been simulated to verify, by comparing the results obtained with the *Friis* transmission equation, the correctness of the gain of the antenna evaluated through near-to-far field transformation. Relative errors on the gain smaller than 3.9% have been reported. The maximum corresponding error in the received power is always smaller than 3.0%. We think that the use of directive nanoantennas could greatly enhance the capability of optical wireless links for on-chip communications. Works are in progress for the design of antenna arrays based on the proposed Vivaldi antenna. The aim is to exploit the increase in gain suited by this configuration to realize longer links for inter- and intra-chip optical communications.

Funding

Ministero dell'Istruzione, dell'Università e della Ricerca (MIUR); PRIN 2015 (20155EABBC).

Acknowledgments

Gaetano Bellanca acknowledges support from "Bando per l'acquisizione di strumenti per la ricerca di Ateneo - Anno 2015" of the University of Ferrara.